3-6 Flight Experiments of Airborne High-Resolution Multi-Parameter Imaging Radar, Pi-SAR

SATAKE Makoto, URATSUKA Seiho, UMEHARA Toshihiko, MAENO Hideo, NADAI Akitsugu, KOBAYASHI Tatsuharu, MATSUOKA Takeshi, MANABE Takeshi, and MASUKO Harunobu

The Polarimetric and Interferometric Synthetic Aperture Radar (Pi-SAR) is an airborne high-resolution imaging radar system, having developed and being operated by Communications Research Laboratory (CRL) and National Space Development Agency of Japan (NASDA). It consists of an X-band synthetic aperture radar and an L-band one, both of those are fully polarimetric and the X-band one has two receiving antennas located in cross-track direction for interferometrc observation. It has been operated for research purposes since 1996, to produce high-resolution polarimetric radar images all over Japan. In this paper we summarize results of Pi-SAR observation experiments, as well as its purposes and future plans.

1 Introduction

The polarimetric and interferometric synthetic aperture radar (Pi-SAR), jointly developed by the Communications Research Laboratory (CRL) and the National Space Development Agency of Japan (NASDA), is an advanced airborne imaging radar system[1][2] featuring high resolution and a variety of advanced functions (e.g., multi-frequency, polarimetric, interferometric observation functions). This radar system is expected to be highly effective in extracting a variety of features of the ground surface. Many sophisticated airborne SAR systems developed worldwide to date are merely prototypes designed to test functions that will be employed in future satellite-borne SAR systems. Pi-SAR, on the other hand, has been developed with emphasis on daily application; it is designed not only for academic applications in such areas as vegeta-tion and oceanography, but also for such practical applications as collecting information during a natural disaster.

Pi-SAR is essentially the only multi-parameter SAR system presently available to domestic researchers. Moreover, it is difficult for the CRL to conduct a wide range of experiments alone. Thus collaboration with external researchers is essential, and a number of intensive Pi-SAR-related joint research projects are underway.

This paper first describes the objectives and methods of Pi-SAR observations and experiments, then discusses some of the obtained experimental results. This discussion will include a summary of experiments jointly conducted with external institutes, as well as the results of performance checks (such as radar calibration) conducted by CRL alone. The last chapter of the paper presents an overall summary and addresses the topic of future

research plans.

2 Objectives of Experiments

The objectives of Pi-SAR observations and experiments are divided into the following three categories:
(1) Evaluation and verification of the basic capabilities of high-resolution, multi-parameter SAR,
(2) Verification of the capabilities of high-resolution, multi-parameter SAR in various applications,
(3) Verification of SAR capabilities in daily applications, such as gathering information in case of emergency.

The Communications Research Laboratory has performed its experiments thus far with goal (1) as a top priority, while at the same time working with external institutions (e.g., universities, national research institutes) toward goal (2). Activities related to goal (3) are performed mainly when large-scale disasters occur. For example, Pi-SAR played an important role in the observation of volcanic eruptions in 2000 (i.e., Mt. Usu, Miyake island), with the cooperation and understanding of both internal and external organizations regarding research funds and aircraft services.

The obtained experimental data is analyzed not only by CRL but also by cooperating external institutions. To make the obtained data widely available, we are constructing a system to distribute this data in several ways: in CD-ROM, in a searchable catalogue-image database, and in dissemination on demand. Furthermore, with respect to the planning of data-collection observations, we are establishing a program for soliciting research ideas from the public to help expand the range of applications in accordance with the above-mentioned policy goals.

Our final goal is to clarify the capabilities and limitations of synthetic aperture radar (SAR) in diverse applications through experiments, observations, and analysis using Pi-SAR data, as we explore new fields of practical SAR application. Our hope is that the SAR system will not only be of use to researchers, but that it will also serve the public at large. Further, we plan to come up with a blueprint for the specifications and development of an advanced SAR that will address its current limitations, as we work to transfer this multi-parameter SAR technology, tested in actual airborne radar experiments, to satellite-borne applications.

3 Experimental Results

This chapter describes the results of Pi-SAR observations and measurements. Table 1 is a summary of the dates and sites of experiments conducted thus far.

3.1 Performance Check

We must ensure that the image data provided by Pi-SAR represents the correct backscattering properties of an observation target, both quantitatively and qualitatively, before using the data for analysis. It is a common practice to check the correlation between the produced image data and a real backscattering coefficient, with reference to a target for which backscattering properties are predictable or already known. This process is referred to as radar calibration. This section describes the calibration experiments of X-band SAR, conducted as part of a series of performance checks. The calibration of L-band SAR is to be carried out by NASDA[3].

3.1.1 Radiometric Calibration

We carried out radiometric calibration with trihedral corner reflectors to clarify the relationship between the obtained image data and backscattering coefficient. Such radiometric calibration will make it possible to compare the obtained data with that of other radar systems on a quantitative basis. The trihedral corner reflector has the advantages of small size, a large backscattering cross section, and a wide beam width (which make it less susceptible to installation-angle errors). Conversely, since it is a point target, there are drawbacks in that the focus is easily blurred by fluctuations in the platform aircraft's orbit

Objective	Date of observation	Path number	Observation site
1. Performance check flight	1996.08.06	2	Noto Peninsula
	1996.08.10	3	Kobe/Awaji
2. L-band calibration	1996.11.19	9	Niigata/Nagano
	1996.11.20	8	Niigata/Nagano
3. Oil spill	1997.01.15	9	Off the coast of Noto Peninsula
(Nakhodka tanker)	1997.01.16	13	Off the coast of Noto Peninsula
4. Observation of sea ice	1997.02.22	6	Okhotsk Sea
	1997.02.23	7	Okhotsk Sea
5. X-band calibration	1997.05.27	10	Tottori/Japan Sea
	1997.05.28	11	Tottori/Osaka
6. Observation of Kanto Area	1997.09.30	12	Tokyo/Tsukuba
	1997.10.01	8	Oze/Nagano/Niigata
7. Observation of sea ice	1998.02.23	11	Niigata/Okhotsk Sea
	1998.02.24	11	Hokkaido/Okhotsk Sea
Exhibit in Haneda	1998.02.25	11	Hokkaido/Okhotsk Sea
	1998.02.26	6	Iwate/Ibaraki/Ohshima
8. X-band calibration	1998.05.26	12	Tottori/Kyoto
	1998.05.27	11	Tottori/Osaka
Kumamoto flight	1998.05.28	11	Hiroshima/Kumamoto
9. X-band calibration	1998.10.22	9	Tottori/Osaka
	1998.10.23	7	Tottori/Kobe
Observation of vegetation	1998.10.26	9	Mt. Iwate, Tomakomai
	1998.10.27	8	Mt. Iwate, Tomakomai
Observation of sea	1998.10.29	6	Kuroshio/Kumamoto/Seto Inland Sea
10. Observation of sea ice	1999.02.23	12	Okhotsk Sea/Tomakomai
	1999.02.24	11	Okhotsk Sea/Tomakomai
11. Summer observation	1999.07.13	8	Kuroshio/Kojima Bay/Nagoya
	1999.07.14	10	Niigata/Tomakomai/Ohgata village
	1999.07.15	1	Mt. Fuji
12. SRTM observation	1999.10.08	11	Kashima calibration
	1999.10.13	16	Mt. Fuji/Tsukuba
	1999.10.14	12	Tomakomai
13. Observation	2000.03.09	10	Okinawa
	2000.03.10	9	Iriomote/Miyako
14. Observation of Mt. Usu	2000.04.06	10	Mt. Usu
	2000.04.12	12	Mt. Usu
	2000.05.30	13	Mt. Usu
15. Observation of Izu Islands	2000.07.06	8	Miyake/Kozu/Ohshima/Hachijo
16. Observation of Mt. Usu and Izu Islands	2000.08.02	10	Mt. Usu/Miyakejima, other areas
17. Observation of Izu Islands	2000.08.30	7	Miyake/Kozu/Ohshima/Hachijo
18. PACRIM	2000.10.01	1	Tsukuba
	2000.10.02	10	Niigata/Usu/Tomakomai/Mt. Iwate
	2000.10.03	8	Mt. Fuji/Nara/Kyoto/Kobe
	2000.10.04	9	Kumano Nada/ Awaji/ Tottori/ Fukuoka
	2000.10.05	7	Unzen/Aso/Sakurajima/Yakushima
19. Miyake emergency observation	2000.10.06	7	Miyakejima/Ohshima
20. Miyake emergency observation	2000.11.12	7	Miyakejima/Ohshima
21. Miyake emergency observation	2001.01.06	12	Miyakejima/Ohshima
22. Miyake emergency observation	2001.01.31	8	Miyakejima/Ohshima/Mt. Fuji
23. Miyake emergency observation	2001.03.01	8	Miyakejima/Ohshima/Mt. Fuji
24. Observation of Tsukuba and Okhotsk Sea	2001.03.02	15	Niigata/Ohgata village/Okhotsk Sea
	2001.03.03	14	Okhotsk Sea/Tsukuba
25. Miyake emergency observation	2001.03.19	8	Miyakejima/Ohshima/Mt. Fuji
26. 2001 1st quarter	2001.08.02	13	Agro-Environment Institute /CRL/Mt. Fuji
27. 2001 2nd quarter	2001.08.29	14	Sado/Ohgata village/Mt. Iwate/Kamaishi
	2001.08.30	13	Sendai/Hatoyama/Mt. Fuji
28. 2001 3rd quarter	2001.11.06	24	Hatoyama/Tokyo Bay/Mt. Fuji
	2001.11.08	14	Kumano Nada/Shikoku/ Kyushu/Okinawa
	2001.11.09	13	Iriomote/Miyako/Ocean radar
	2001.11.10	15	Okinawa/Amami Islands/ Kyushu/Chugoku/Gifu

Table 1 Pi-SAR experiments (August 1996 to October 2001)

and attitude. Moreover, unless the gain of input to the radar receiver is appropriately controlled, the receiver input level will become saturated and the detectable backscattering power from the point target will decrease when radar imaging data is created. For precise measurement of the backscattering power returned from the point target, the background of the target-installed site must be uniform over a wide range and feature a small backscattering coefficient. In general, dry, sandy surfaces feature relatively low backscattering coefficients. We chose Tottori Dune in Japan as a site that met the necessary requirements, and installed corner reflectors there for calibration experiment.

Fig.1 shows the images obtained in a calibration experiment conducted in October 1998, along with locations of installed corner reflectors. In Fig.2, the backscattering power estimated from the image data provided by the corner reflectors is plotted on the vertical axis, with the calculated backscattering cross section plotted on the horizontal axis. The values for X-band radiometric calibration were determined from this figure[4].

3.1.2 Polarimetric Calibration

One of the advantages of Pi-SAR lies in its ability to perform polarimetric observation using two orthogonal linear (horizontally and vertically) polarized waves. However, because the raw data obtained by the observation usually contains cross-talk and features an imbalance between the polarimetric channels, it does not provide precise information regarding polarimetric properties. Our polarimetric calibration experiment for evaluating and correcting such cross-talk and channel imbalance are described below.

Because the common trihedral corner reflector employed in normal radiometric calibration returns only co-polarized wave (i.e., horizontally polarized wave when the horizontally polarized wave is incident), it alone cannot provide data for polarimetric calibration. Consequently, another type of reflector is needed to return cross-polarized components. Thus, we prepared special dihedral corner
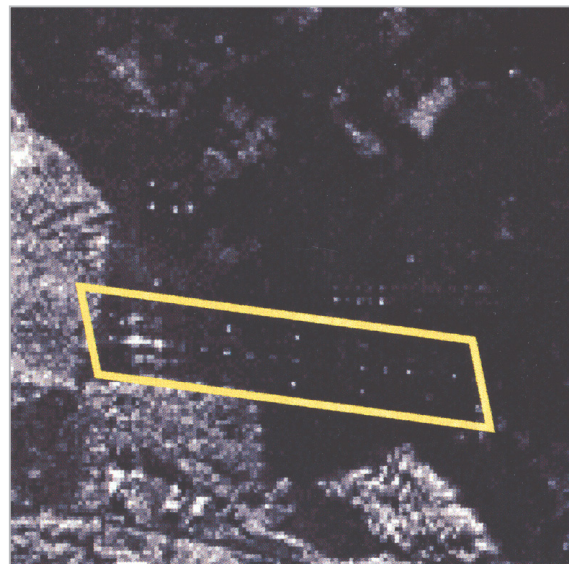

Fig.1 Images of corner reflectors deployed on Tottori Dune for radiometric calibration experiment (X-band, VV mode, flight direction , illumination direction)
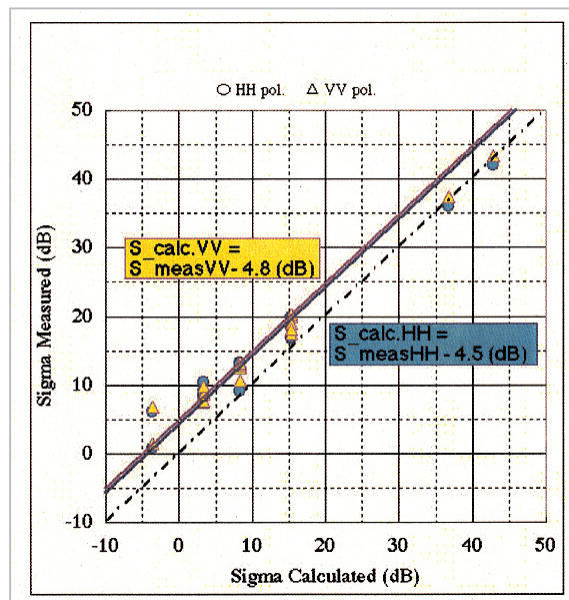

Fig.2 Backscattering power from corner reflectors: Measurement and calculation

reflectors for this purpose. A 45 °-rotated dihedral corner reflector [Fig.3 (a)] around the axis connecting the radar and reflector returns only the cross-polarized component (i.e., vertically polarized wave when horizontally polarized wave is incident, and vice versa). A 22.5 °-rotated dihedral corner reflector [Fig.3 (b)] returns the co-polarized component and cross-polarized component evenly (i.e., hori-
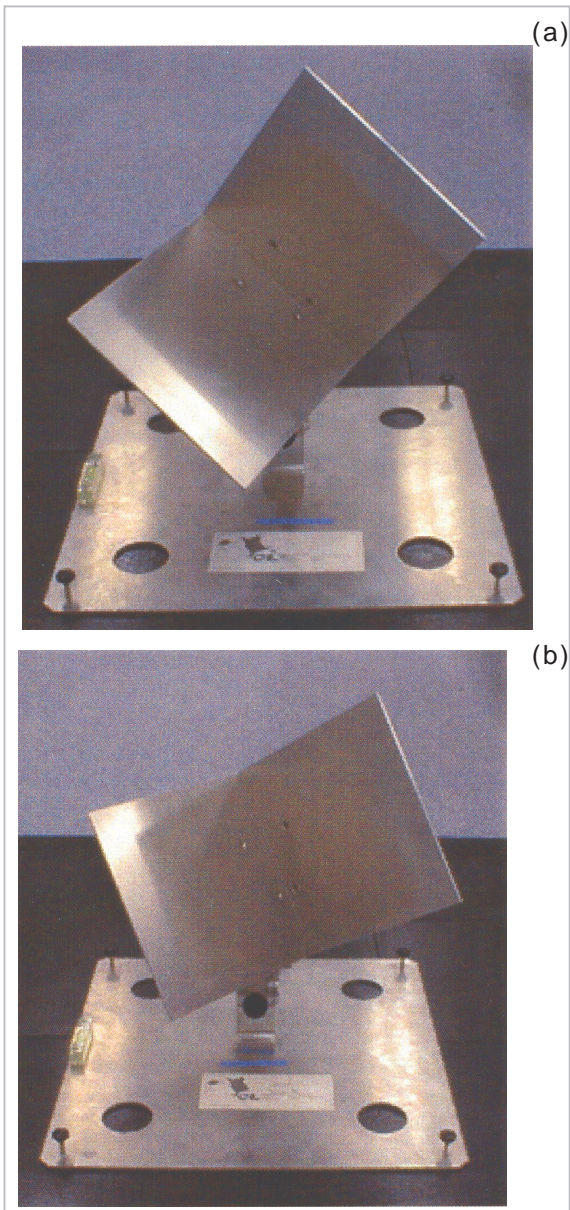
(a)

(b)

Fig.3 (a) 45°-rotated dihedral corner reflec-
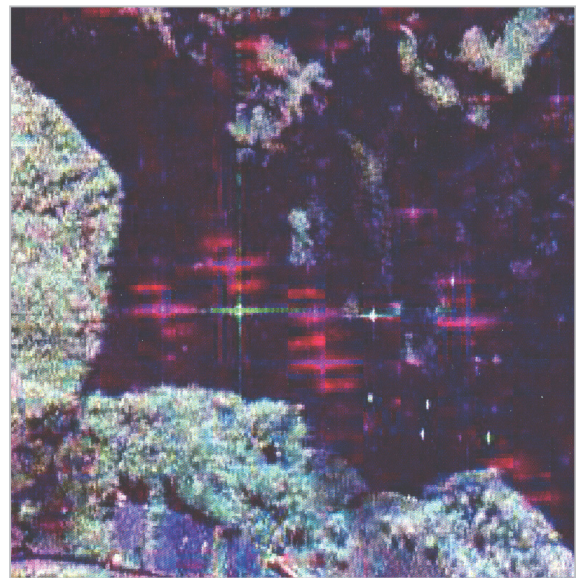tor,
(b) 22.5°-rotated dihedral corner
reflector

Fig.4 Images of corner reflectors installed on
Tottori Dune for polarimetric calcula-
tion experiment (X-band, polarimetric
composite color image (HH: red, HV:
green, VV: blue), flight direction , illu-
mination direction)

zontal and vertical waves when horizontal
wave is incident). Fig.4 demonstrates the
detected image of the corner reflectors
installed at Tottori Dune. Data analysis for
polarimetric calibration is currently underway
[5].

3.2 Application Experiment

Described below are representative Pi-
SAR application experiments, organized by
the respective fields of application.

3.2.1 Urban Areas

For the observation of urban areas, high
resolution of the X-band SAR (1.5 m) is par-
ticularly useful. Images of the Imperial Palace
and Tokyo Station shown in Fig.5 offer a kind
of perspective view provided by the "Lay
Over" effect by which the upper parts of high-
rise buildings near Marunouchi are casted
toward the radar in the picture. Visualization
of these building structures using high-resolu-
tion SAR represents a future subject, where
the dependence on materials, shapes, and
directions should be clarified.

With regard to the examples of earth-
quake-risk management in urban areas using
remote-sensing techniques, a trial program[6]
is currently underway to analyze downtown
structures based on Pi-SAR data.

3.2.2 Forest

Fig.6 (a) is a colored elevation profile of a
national forest in Tomakomai, drawn based on
the differential phase data acquired in October
2000 using the Pi-SAR in interferometry
mode. Fig.6 (b) represents the elevation pro-
file across the white line in Fig.6 (a). Most of
the X-band radio waves illuminated to a forest
are likely to be backscattered by the tops of
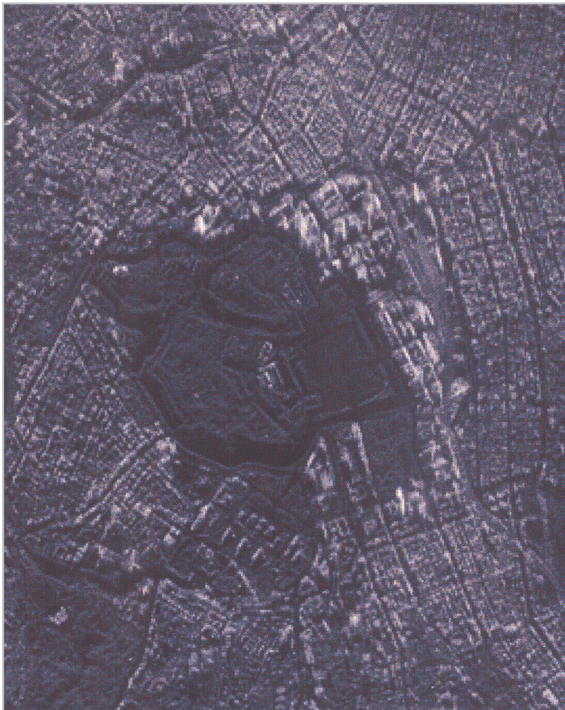the trees. Thus the height of a forest may be

Fig.5 Images of Imperial Palace and vicinity (X-band, HV polarization, flight direction ,) illumination direction)
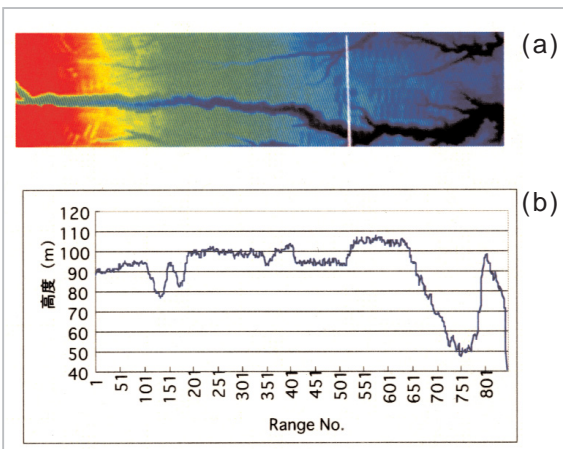

Fig.6 Forest observation in Tomakomai : (a) topographic image created from interferometry observation (X-band, High: red, Low: blue), (b) elevation profile along white line on (a)

estimated using Pi-SAR. X-band and L-band polarimetric observations are performed in parallel to identify different species of trees. The biomass of the forest may be estimated provided an appropriate model is established. This biomass information is essential for the estimation of forest resources and amount of fixed carbon dioxide in the atmosphere. In connection with these analyses, we have measured the heights and diameters of trees from ground level[7][8].

3.2.3 Agricultural Products

Fig.7 (a) and (b) show X-band and L-band images of a farm in Ohgata village, Akita Prefecture, taken in July 1999. These represent color-enhanced images where the backscattering intensities in polarization channels-HV, VV and HH are scaled to an RGB color composite. Fig.7 (c) is a crop map of the same farm. A comparison of these microwave maps with the crop map shows that paddy fields (occupying most of the farm) are clearly distinguished from the other crop fields based on information relating to the X-band HH/VV polarimetric ratio[9]. Moreover, the visualized color images of the polarimetric data differ according to crop species (e.g., barley, soy bean) on the farm, which suggest that multi-frequency, polarimetric observation is useful in identifying crop species. Of note in such airborne radar-based observation is that the incident angles on the ground differ between the near side (closest to the aircraft or top side of the figure) and the opposite, far side (at the bottom of the figure), and that image intensity depends greatly on the incidence angle of radar waves.

In addition, rice crop observational research is in progress over reclaimed land in Kojima Bay, Okayama Prefecture[10][11], representing another multi-frequency, polarimetric Pi-SAR observation application.

3.2.4 Sea Ice

We observed sea ice in the winters of 1998, 1999, and 2001 off the eastern coast of Hokkaido in the Okhotsk Sea. Fig.8 is a composite color image of the X-band and L-band in which polarimetric images acquired in February 1999 are overlapped. During this observation, conducted in collaboration with Hokkaido University and others, we employed sonar to measure the thickness of ice (ice draft). As a result, we found a strong correlation between the backscattering coefficient of the L-band, cross-polarized component (HV) and ice thickness [see Fig.8 (a)]. In addition, we found that it was possible to detect areas of
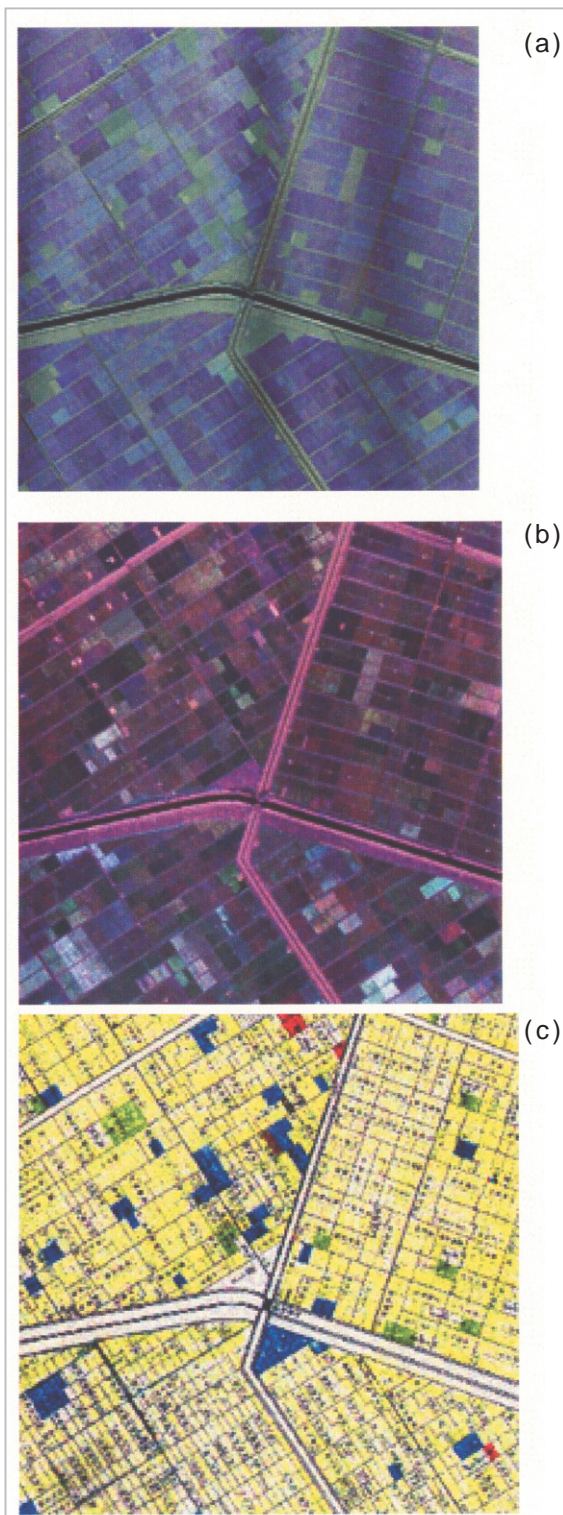
band differential reflectivity horizontal/vertical polarization ratio (VV/HH) [Fig.8 (b)][1 2][1 3].

3.2.5 Ocean

Researchers have focused on ocean waves as potential targets of SAR-based sea observation. However, conventional SAR features a spatial resolution of 10 m or lower, and is therefore only useful for observations focusing on relatively long waves; in other words, conventional SAR cannot provide sufficiently short data intervals when investigating spatial changes in sea waves.

Pi-SAR, which features high spatial resolution, allows sea-wave observation featuring high precision and spatial density over a wide range of sea-wavelengths.

In measurements over a path across the Kuroshio conducted out in 1998 and 1999, spatial changes in the ocean-wave spectrum (Fig.9) caused by the Kuroshio were successfully observed.

3.2.6 Paleo-environment

As in the case in which the Shuttle Imaging Radar found an ancient waterway buried underground, our SAR observation is also expected to provide information about paleo-environment, utilizing the penetrating capabil-
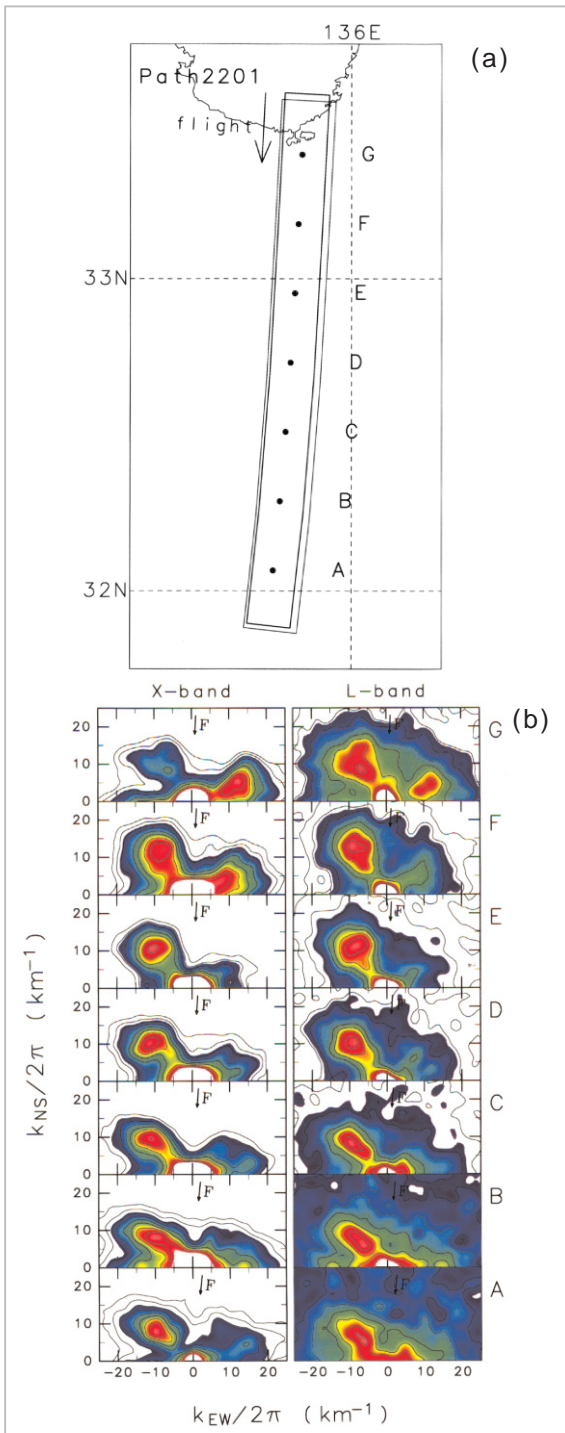
thin ice (10 cm or thinner) that play a key role in heat exchange between the atmosphere and the sea. This was done using the obtained X-

(a)

(b)

Fig.9 *Observation of Kuroshio off Wakaya-ma coast : (a) range of observation, (b) spatial change in ocean-wave spectra provided by SAR data*
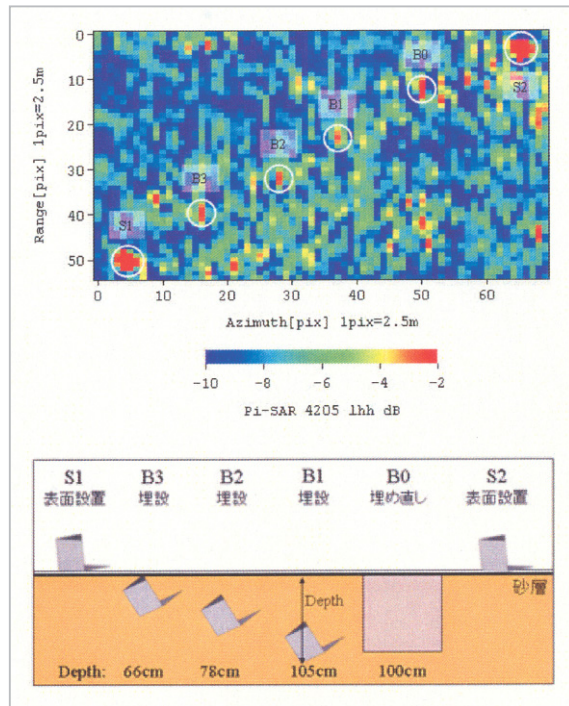

Fig.10 *Experimental detection of buried objects (L-band, VV polarization)*

Pi-SAR to this field of research, we attempted to detect sample objects buried in Tottori Dune. Fig.10 shows an example of their L-band VV images. Analysis of the data indicated that variations in the backscattering intensity of returned waves were due to variable radio-wave decay in the sand attributable to the placement of objects buried at different depths[14].

3.3 Program Experiment

With Pi-SAR as our tool, we joined an imaging radar program hosted by the National Aeronautics and Space Administration (NASA) and the Deutsche Zentrum fur Luft-und Raumfahrt (DLR).

3.3.1 Conjunctive observation with the Shuttle Radar Topography Mission

We observed Mt. Fuji and Tomakomai with the Pi-SAR in October 1999, in connection with the Shuttle Radar Topography Mission (SRTM) using the space shuttle-borne SAR. Fig.11 shows the image of Mt. Fuji and topographic profile created from interferometric observation data. For this observation of Mt. Fuji, we installed corner reflectors at a few sites of known elevation in advance to
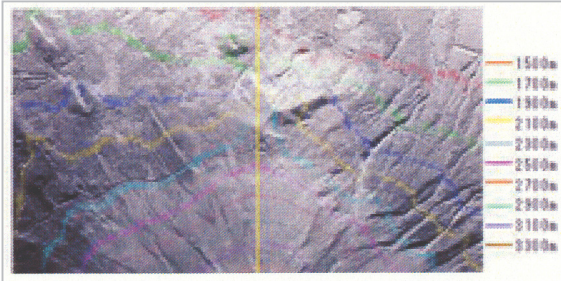
ity of radio waves. Particularly in dry, sandy areas, microwaves easily penetrate the ground, revealing intriguing information about underground structures.

As a preliminary experiment in adapting

Fig.11 Observation of Mt. Fuji using X-band Pi-SAR, amplitude image (VV polarization) overlapped onto contour profile provided by interferometry observation
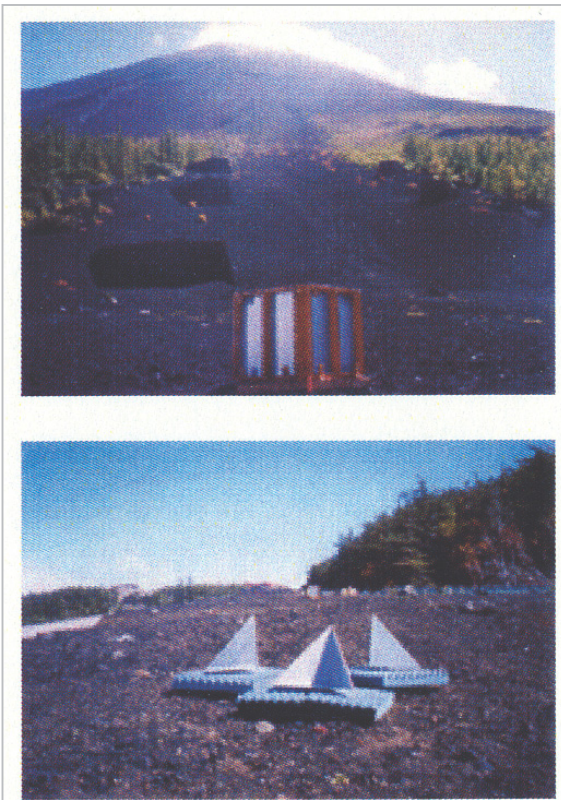

Fig.12 Installation of corner reflectors for Mt. Fuji profile mapping experiment (photo)
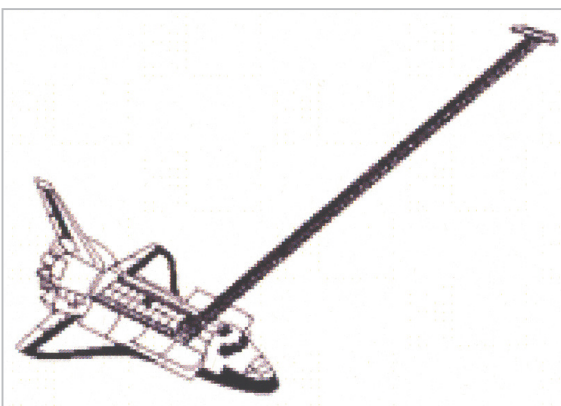

Fig.13 Schematic drawing of antenna used in SRTM experiment

establish reliable verification data (Fig.12).

The space shuttle flight itself was postponed until February 2000 due to technical problems. The aim of the SRTM was to acquire elevation maps of virtually the entire surface of the Earth through interferometry observations using the space shuttle-borne X-band SAR main antenna and a secondary antenna installed about 60 m from the main antenna, as shown in Fig.13. CRL was selected as a research partner of the DLR, which had participated in the SRTM together with the Jet Propulsion Laboratory (JPL) of the United States. The DLR is scheduled to provide CRL with X-band digital elevation model (DEM) data and image data of 20 km swath. The experiment we proposed with respect to the creation of DEM by SRTM (X-band) was designed to investigate the following by using Pi-SAR: (1) disagreement between the high-resolution DEM data by Pi-SAR and the DEM by SRTM (X-band); (2) influence of the local incident angle at slopes; and (3) influence of vegetation on the resulting image[15].

3.3.2 Observation in conjunction with AIRSAR

We conducted Pi-SAR observations in October 2000 (Fig.14), in connection with the Pacific Rim Mission (PacRim2) campaign, in which JPL's AIRSAR observed Japanese land areas. AIRSAR and Pi-SAR observed about 30 experimental sites in Japan over the course of two days and five days, respectively. In connection with this experimental program, we urged domestic researchers to join in intensive efforts to collect ground data.

One of the objectives of joint observation with AIRSAR was to conduct polarimetric observation using multi-frequency microwaves in the P, L, C, and X bands during a single test period. Data acquired with microwaves from the P to X bands, each with its own penetration characteristics relative to terrestrial objects, will undoubtedly prove extremely useful for analysis of an area composed of elements of various sizes, such as a forest. Conversely, we had to avoid interference with existing domestic radio stations that

use the P band during our P-band experiment. Thus we limited the experimental sites to Tomakomai and Tottori. The P-band experiment conducted in Tomakomai represented the application of the P-band to the measurement of forests and vegetation. The P-band measurement in Tottori Dune was intended to locate objects buried in sand. Since the L-band was used both by AIRSAR and Pi-SAR, cross-referenced data will allow for mutual calibration. We expect that this data will enable precise comparison between two SAR (AIRSAR and Pi-SAR) data sets, gathered at different times from different sites[16]. Fig.15 shows the images of the corner reflectors provided by (a) AIRSAR and (b) Pi-SAR.

3.4 Emergency Observation During Disasters

The results of emergency observations and experiments conducted during natural and man-made disasters are described below, in applications where airborne SAR was able to play a key role thanks to its mobility and all-weather operability. To act quickly for conducting emergency observations, we built facilities to house the Pi-SAR system on the premises of an aircraft service company near Nagoya Airport in 2000. As a result, the time that would have been required for transportation from CRL (i.e., previous site of Pi-SAR's facilities) to Nagoya Airport was saved; speedier and more flexible observation was thus made possible.

3.4.1 Oil spill: Nakhodk accident in the Japan Sea

A Russian tanker sank in the Japan Sea in January 1997, resulting in spillage of crude oil into the sea. CRL and NASDA conducted emergency observations using Pi-SAR to observe the spread of oil on the surface off the coast of Ishikawa Prefecture. Spilled oil on the sea surface inhibits the generation of surface waves; SAR thus returns a dark image of the affected area, as the backscattering coefficient here is less than that of the non-affected area[17]. As shown in Fig.16, the area contaminated with oil in the accident presented a

Fig.14 AIRSAR and Pi-SAR on standby at Nagoya Airport for PacRim2 mission
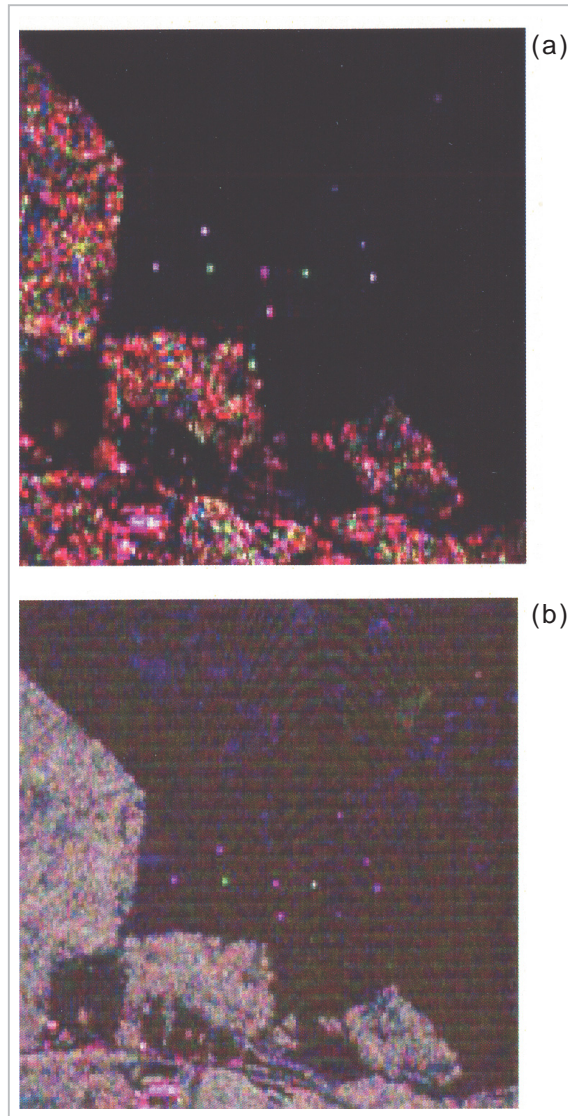

(a)

(b)

Fig.15 Images of L-band corner reflectors installed on Tottori Dune for PacRim2 mission : (a) AIRSAR and (b) Pi-SAR both use L band, polarimetric composite color image (HH: red, HV: green, VV: blue), flight direction , illumination direction

Fig.16 *Image of crude oil spilled from Nakhodka tanker (L-band, VV polarization, off the coast of Noto Peninsula)*

backscattering coefficient less than that of its surroundings, and was thus observed by Pi-SAR.

3.4.2 Volcanic disaster I: Mt. Usu in Hokkaido

Mt. Usu in Hokkaido erupted at the end of March 2000. We observed the formation of craters and faults near Mt. Konpira and the Nishi-yama area on April 6, April 12, and May 30. Optical systems are normally useless in the observation of volcanic disasters because visibility is impaired by volcanic smoke and clouds. Conversely, microwaves are not affected by these obstructions and thus continuous observation is possible.

Fig.17 shows the X-band polarimetric composite color images observed on April 6 and 12. The differences in color tone are explained as follows: In general, the cross-

polarized component (HV) is returned from objects with complex shapes, such as plants. This is reflected in the strong presence of green elements. Meanwhile, urban buildings and objects having simple shapes return strong co-polarized elements (HH + VV) and are represented by purple-enhanced colors (red + blue). The purple image near the crater can be attributed to vegetation covered with volcanic ash. It is possible to estimate the shape, dimensions, and position of the crater from the image, and we can note changes between the two periods of observation. Numerous streaks are seen in the east-west direction near the craters on the west side of Nishi-yama. These streaks can be attributed to faults and cracks resulting from tectonic movement. Furthermore, a spreading of the mud stream generated on April 10 is recognized on the north side of Mt. Konpira, as indicated by color tone changes in the polarimetric images[18]. We estimated the ground height changes both upward and downward caused by tectonic movement based on the interferometry data acquired over the three observation periods mentioned above. As a result, upheavals of up to about 30 m were identified[19].

3.4.3 Volcanic Disaster II: Miyake Island

The volcanic activities of Miyake Island increased markedly in late June 2000, and there was a massive eruption on July 8, followed by collapse of the crater. Volcanic activity has continued since then and all residents were forced to evacuate from the island. Pi-SAR made emergency observations on August 2, August 30, October 6, and November 12, 2000, and on January 31, March 2, and March 19 of the following year.

Fig.18 (a) (July 6 data initially acquired in the series of Miyake Island observations) shows the island image immediately before the large-scale collapse. A flat caldera was seen near the top of Oyama in the center of Miyake Island. Fig.18 (b) (August 2) clearly shows the collapse of the caldera at the top of Oyama. Typical imaging radar systems observe the ground from the top in a slanting

Fig.17 Observation of Mt. Usu eruption (X-band, polarimetric composite color image (HH: red, HV: green, VV: blue), flight direction , illumination direction), (a) April 6, 2000, (b) April 10, 2000

Fig.18 Observation of Miyake Island eruption (X-band, polarimetric composite color image (HH: red, HV: green, VV: blue), flight direction , illumination direction), (a) July 6, 2000, (b) August 2, 2000

direction. Thus, if there is a steep slope, the region where microwaves do not reach appears black (like a shadow). This is why most parts of the crater appear black. It is possible to estimate the depth of the crater from the length of shadow in the figure, and we determined that this value was 410 m[20]. Fig.19 shows the altitude profile of the crater,
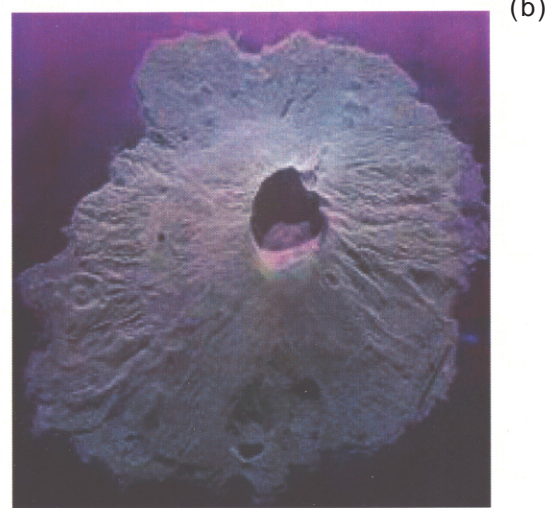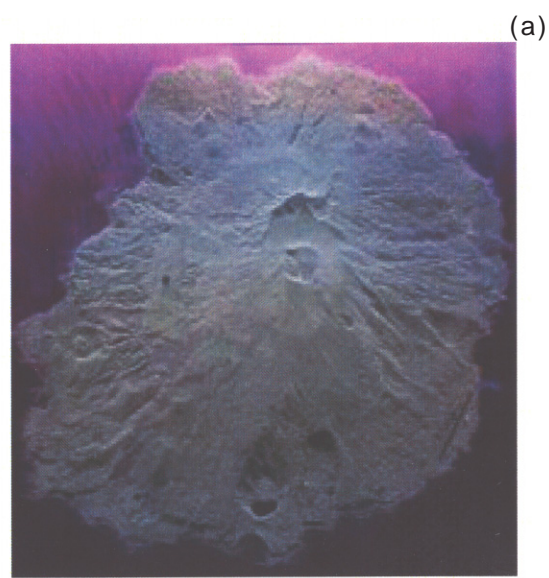
which was estimated from the interferometry data obtained on those observation days. This figure indicates that the large-scale ground collapse occurred between July 6 and August 2; later, the south side of the crater fell further (by August 30), with virtually no change after that time. In addition, this data indicates that the incline of the crater is approximately 45 degrees.
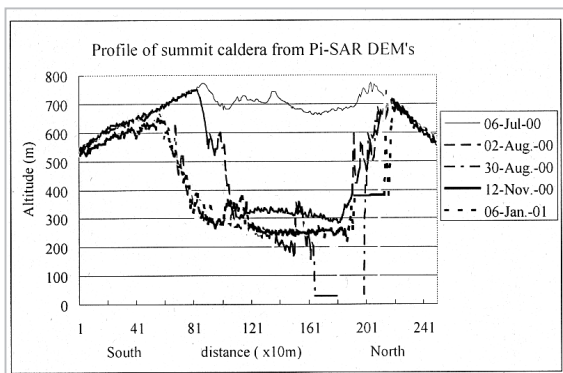
4 Future Plan

Fig.19 *Altitude profile of vicinity of the caldera of Miyake Island (Oyama) provided by interferometric measurement*

As mentioned above, Pi-SAR collected high-resolution polarimetric image data over a number of sites in Japan through a series of aircraft observation. It also gathered data relating to the volcanic activity of Mt. Usu and Miyake Island on a continual basis. Pi-SAR is expected to continue its aircraft observation, and we will continue to analyze the obtained data to ensure the effectiveness of SAR-based environmental measurement and disaster monitoring.

Preparations are currently underway for a new stage of experiments, with priority placed on the following three activities:

(A) We will publicly solicit ideas for Pi-SAR observations in order to extend the range of our imaging radar research and to encourage the effective use of the data obtained.

(B) Through Pi-SAR overseas observations, we will collect data for geotechnical investigation and paleo-environment exploration that is difficult to collect in Japan.

(C) In connection with the phased-array L-band SAR (PALSAR) to be boarded on the advanced land observation satellite (ALOS) scheduled for launch by NASDA in 2004, we will push forward all relevant research activities, including cross-calibration of PALSAR and Pi-SAR.

5 Conclusions

Pi-SAR has collected imaging radar data from a number of locations across Japan since its first flight test in 1996. The obtained data, representing Japan's first high-resolution polarimetric image data, has provided useful information for investigators involved in SAR application research. We have also provided image data that has proven useful in understanding the conditions surrounding natural disasters. To cite two examples, Pi-SAR served as an airborne imaging radar system, gathering information on a continual basis when Mt. Usu and Miyake Island experienced volcanic activity. Thus observers were able to take advantage of the all-weather availability and portability of Pi-SAR. We intend to continue experiments relating to Pi-SAR applications and expand its range to encompass more extensive environmental measurements and disaster-monitoring activities, through collaboration with researchers at external institutions.

References

1 T. Kobayashi, et al., "Airborne Dual-Frequency Polarimetric and Interferometric SAR", IEICE Trans. Commun., Vol. E83-B, pp. 1945-1954, 2000.

2 T. Umehara, et al., "Development of airborne high-resolution multi-parameter imaging radar SAR, Pi-SAR", This Special Issue of CRL Journal.

3 H. Wakabayashi, et al., "Cross-calibration experiment of airborne L-band SAR", Proc. 30th Conf. of Remote Sensing Society of Japan, pp.261-262, Apr. 2001. (In Japanese)

4 M. Satake, et al., "Calibration of an X-band Airborne Synthetic Aperture Radar with Active Radar Calibrators and Corner Reflectors", CEOS 1999 SAR Workshop, Toulouse, France, 1999.

5 M. Satake, et al., "Development of Polarization Selective Corner Reflectors and Its Experiments for Calibration of Airborne Polarimetric Synthetic Aperture Radar", IEEE 2001 International Geoscinece

and Remote Sensing Symposium, Sydney, Australia, 2001.

6 H. Aoki, et al., "Backscattering characteristics of airborne SAR images for seismic vulnerability assessment in urban areas", 20th Asian Conf. Remote Sensing, Hong-Kong, 1999.

7 M. Suginaka, et al., "Evaluation of SAR forest observation by laser scanner", Proc. 29th Conf. of Remote Sensing Society of Japan, pp.51-52, Nov. 2000. (In Japanese)

8 N. Mitsuzuka, et al., "Specific characteristics of forest observation data by high resolution/full polarimetric airborne SAR", Journal of Remote Sensing Society of Japan, Vol.20, No.4, pp.47-66, 2000. (In Japanese)

9 T. Umehara, et al., "The observation of vegetation by airborne SAR (PI-SAR)", Proc. 27th Conf. of Remote Sensing Society of Japan, pp.203-204, Nov. 1999. (In Japanese)

10 N. Ishitsuka, et al., "Next SAR specification at terrestrial ecosystem observation Kojima reclaimed land observation project of various SAR", Proc. 27th Conf. of Remote Sensing Society of Japan, pp.155-158, Nov. 1999. (In Japanese)

11 N. Ishitsuka, et al., "Observation of the rice paddy fields using polarimetric data by Pi-SAR", Proc. 32nd Conf. of Remote Sensing Society of Japan, pp.29-30, May 2002. (In Japanese)

12 T. Matsuoka, et al., "Deriving sea ice thickness and ice types in the Sea of Okhotsk using dual-frequency airborne SAR (Pi-SAR) data", Annals of Glaciology, Vol. 34, to be published.

13 T. Matsuoka, et al., "CRL/NASDA airborne SAR (Pi-SAR) observations of sea ice in the Sea of Okhotsk", Annals of Glaciology, Vol. 33, pp115-119, 2001.

14 H. Honma, et al., "Scattering model for buried object in sand validated by two airborne SAR data", Proc. 31th Conf. of Remote Sensing Society of Japan, pp.127-128, Dec. 2001. (In Japanese)

15 S. Uratsuka, et al., "Evaluation experiments for X-SAR/SRTM by airborne SAR (PI-SAR)", Proc. 27th Conf. of Remote Sensing Society of Japan, pp.167-168, Nov. 1999. (In Japanese)

16 S. Uratsuka, et al., "Preliminary results of the Pacific Rim 2000 campaign in Japan", Proc. 29th Conf. of Remote Sensing Society of Japan, pp.269-270, Nov. 2000. (In Japanese)

17 M. Fujita, et al., "SIR-B experiment in Japan: Sensor calibration and oil pollution detection over Ocean", IEEE Trans. Geosci. and Remote Sens., Vol. 24, pp.567-574, 1986.

18 S. Uratsuka, et al., "Preliminary results of airborne SAR (Pi-SAR) observation of Usu Volcano, Hokkaido", IEICE Trans. Commun., Vol.J84-B, No.1, pp.134-136, Jan. 2001. (In Japanese)

19 H. Maeno, et al., "Extraction of crust movements around the crater of Mt. Usu using DEM of Pi-SAR", Proc. 30th Conf. of Remote Sensing Society of Japan, pp.165-166, 2001. (In Japanese)

20 S. Uratsuka, et al., "Volcanic disaster monitoring of Mt. Usu and Miyake Island by high-resolution airborne imaging radar", pp. 23-28, Proc. 99th CRL Symposium, Nov. 2000. (In Japanese)
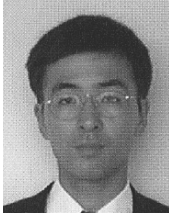
SATAKE Makoto

Senior Researcher, Environment Information Technology Group, Applied Research and Standards Division

Microwave Remote Sensing

URATSUKA Seiho, Dr.Eng.

Leader, Environment Information Technology Group, Applied Research and Standards Division
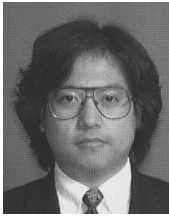
Microwave Remote Sensing

UMEHARA Toshihiko

Senior Researcher, Environment Information Technology Group, Applied Research and Standards Division

Global Environment Remote Sensing

MAENO Hideo

Senior Researcher, Environment Information Technology Group, Applied Research and Standards Division
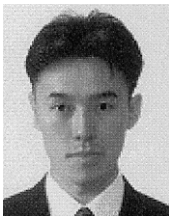
Pi-SAR, Remote Sensing

NADAI Akitsugu

Senior Researcher, Environment Information Technology Group, Applied Research and Standards Division
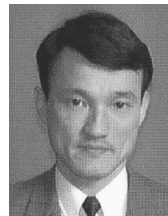
Physical Oceanography, Ocean Remote Sensing

KOBAYASHI Tatsuharu, Dr. Sci

Senior Researcher, Environment Information Technology Group, Applied Research and Standards Division

Microwave Remote Sensing

MATSUOKA Takeshi, Ph.D.

Researcher, Subtropical Environment Group, Applied Research and Standards Division

Radar Remote Sensing, Glaciology

MANABE Takeshi, Dr. Eng.

Leader, SMILES Group, Applied Research and Standards Division

Microwave and Millimeter-Wave Propagation and Remote Sensing

MASUKO Harunobu, Dr. Sci.

Executive Director, Applied Research and Standards Division

Microwave Remote Sensing